

# Volatility Clustering in Medical Ultrasound Imaging and System Identification Based Deconvolution

Kyriaki Kostoglou<sup>1</sup>, Christian Wallinger<sup>2</sup>, Mario Huemer<sup>1</sup>

<sup>1</sup> Institute of Signal Processing, Johannes Kepler University, Linz, Austria

<sup>2</sup> GE Healthcare, Zipf, Austria

**Abstract**—We propose a system identification based deconvolution algorithm for medical ultrasound imaging enhancement. Deconvolution is realized using Multivariate Autoregressive (MVAR) models taking into account the heteroscedastic nature of the recorded ultrasonic signals. Based on simulations, phantoms and in vivo data we show the superiority of the proposed algorithm under the presence of volatility in the obtained images.

**Keywords**—heteroscedasticity, volatility, ultrasound imaging, system identification, deconvolution, multivariate autoregressive

## I. INTRODUCTION

Medical ultrasound is a non-invasive imaging technique that uses high-frequency sound waves to create real-time images of the human body. The procedure involves an ultrasonic probe that transmits short acoustic waves and records the echoes that are reflected back from targeted organ structures. These echoes are then used to produce images of the underlying anatomy. The interaction between the acoustic wave generated by the probe and the scanned human tissue introduces blurring to the output image, reducing both contrast and resolution. Based on physical models, this interaction can be described as the convolution between a tissue reflectivity signal and the emitted ultrasonic pulse. Various blind deconvolution methods have been proposed so far for recovering the true underlying reflectivity function (TRF) from the obtained radiofrequency (RF) signals. However, very few are based on system identification approaches [1]–[5] mainly due to the absence of a real input/excitation (i.e. only the output – obtained image – is known). In addition, computational complexity along with inherent difficulties related to model order selection and parameter estimation discourage the use of system identification techniques. Some of these difficulties arise due to the nonstationary characteristics of the recorded RF signals. RF signals exhibit volatility clustering (i.e., heteroscedasticity) or else highly concentrated variance in specific time points that may affect model order selection and estimation [6]. Heteroscedasticity may arise due to variations in the mean scattering/reflection strength of different types of tissue or due to the ultrasonic device and the beam profile of the transducer.

Herein, we propose a fast and efficient deconvolution algorithm based on Multivariate AutoRegressive (MVAR) models and applied on In-Phase & Quadrature (IQ) data. Typically, the recorded RF signals are real-valued. Nonetheless, this work is based on complex IQ data. IQ data has lower

sampling rate compared to RF data leading to decreased runtime when processing is involved. Based on our proposed methodology, each line of the IQ image is modeled as a 2D AR process, i.e., as an output of a linear filter driven by white Gaussian noise. The 2D refers to the real and imaginary components of each line. We show based on simulations how model order selection/estimation and deconvolution, is affected when the process is driven by heteroscedastic noise, and we propose methods to mitigate its effects. To demonstrate the superiority of the proposed algorithm, deconvolution is applied on phantom and in vivo data.

## II. METHODOLOGY

### A. Multivariate Autoregressive (MVAR) Model

An  $M$ -dimensional MVAR model of order  $p$ , denoted as MVAR( $p$ ) can be expressed as follows [7]

$$\mathbf{y}(n) = \sum_{k=1}^p \mathbf{A}_k \mathbf{y}(n-k) + \boldsymbol{\varepsilon}(n) = \mathbf{A} \boldsymbol{\varphi}(n) + \boldsymbol{\varepsilon}(n), \quad (1)$$

where  $\mathbf{y}(n) \in \mathbf{R}^{M \times 1}$  contains the values of all  $M$  time-series at time  $n$ . Herein,  $M = 2$  and  $\mathbf{y}(n)$  is a vector that consists of the real ( $\mathbf{y}_R$ ) and imaginary ( $\mathbf{y}_I$ ) parts of the IQ data at time  $n$ , i.e.,  $\mathbf{y}(n) = [\mathbf{y}_R(n) \ \mathbf{y}_I(n)]^T$ .  $\mathbf{A}_k \in \mathbf{R}^{M \times M}$  is an autoregressive matrix for each order  $k$  and  $\boldsymbol{\varepsilon}(n)$  is a zero-mean white noise vector.  $\mathbf{A} = [\mathbf{A}_1 \ \dots \ \mathbf{A}_p] \in \mathbf{R}^{M \times Mp}$  and  $\boldsymbol{\varphi}(n) = [\mathbf{y}(n-1)^T \ \dots \ \mathbf{y}(n-p)^T]^T \in \mathbf{R}^{Mp \times 1}$ . The total number  $d$  of model coefficients is equal to the number of elements in  $\mathbf{A}$  and therefore  $d = M^2 p$ . In matrix form, (1) can be written as

$$\mathbf{Y} = \mathbf{A} \boldsymbol{\Phi} + \mathbf{E} \quad (2)$$

$\mathbf{A}$  can be estimated using the Least Squares approach [7],

$$\hat{\mathbf{A}} = \mathbf{Y} \boldsymbol{\Phi}^T (\boldsymbol{\Phi} \boldsymbol{\Phi}^T)^{-1} \quad (3)$$

The estimated  $\hat{\mathbf{Y}}$  is  $\hat{\mathbf{Y}} = \hat{\mathbf{A}} \boldsymbol{\Phi}$ . In order to compute  $\hat{\mathbf{A}}$  though, one needs first to select an appropriate MVAR model order. A large  $p$  value leads to overly complex models that lack the ability to generalize. On the other hand, a small  $p$  may produce rigid and inflexible models that are unable to capture accurately the underlying system characteristics. One method to overcome this problem, is the use of model order selection criteria such as the Bayesian Information Criterion (BIC) [8]. BIC tries to achieve a balance between model fitness and complexity. For each  $p$  value, the multivariate BIC is defined as [9], [10]

$$BIC(p) = N \log(|\hat{\boldsymbol{\Sigma}}|) + d \log(N), \quad (4)$$

where  $N$  is the number of samples,  $d = M^2 p$  is the total number of coefficients and  $|\hat{\boldsymbol{\Sigma}}|$  is the determinant of the estimated residual covariance  $\hat{\boldsymbol{\Sigma}} = \text{cov}(\mathbf{Y} - \hat{\mathbf{Y}}) = \text{cov}(\hat{\mathbf{E}})$ . The

optimal  $p$  is the one that returns the lowest BIC score.

MVAR models can be used to simultaneously extract the Z-transform of the emitted pulse (based on  $\hat{\mathbf{A}}$ ), as well as the underlying reflectivity function [1]–[3]. Once the MVAR model order is determined, the autoregressive matrix  $\mathbf{A}$  is estimated using (3). The MVAR residuals and therefore the wanted deconvolved signals are given as

$$\hat{\mathbf{E}} = \mathbf{Y} - \hat{\mathbf{Y}} = \mathbf{Y} - \hat{\mathbf{A}}\Phi \quad (5)$$

### B. Effect of Heteroscedasticity

MVAR estimation typically assumes that the process is driven by white noise (i.e.  $\boldsymbol{\varepsilon}$ ), with zero mean and constant variance (homoscedastic). However, the IQ data can be highly heteroscedastic and this may affect the model determination and estimation procedure [6]. Based on (4),  $\hat{\boldsymbol{\Sigma}}$  is an estimate of the global residual covariance, and therefore model selection is achieved by taking into account equally all  $N$  samples. Under heteroscedasticity, however,  $\boldsymbol{\Sigma}$  is no longer constant throughout time. The global estimate  $\hat{\boldsymbol{\Sigma}}$  is thus dominated by the residuals with large variance, and model order selection is determined mainly by the respective samples. To this end, we remove the source of heteroscedasticity by tracking the time varying variance of both the real and imaginary components of each IQ line using an exponential moving average,

$$\hat{\sigma}_{R_l}^2(n) = \lambda \hat{\sigma}_{R_l}^2(n-1) + (1-\lambda)y_{R_l}^2(n-1), \quad (6a)$$

$$\hat{\sigma}_{I_l}^2(n) = \lambda \hat{\sigma}_{I_l}^2(n-1) + (1-\lambda)y_{I_l}^2(n-1), \quad (6b)$$

where  $l$  corresponds to the  $l^{\text{th}}$  line. The real and imaginary components are normalized at each time point  $n$  as

$$y_{R_{l_{\text{new}}}}(n) = \frac{y_{R_l}(n)}{\sqrt{\hat{\sigma}_{R_l}^2(n)}}, \quad y_{I_{l_{\text{new}}}}(n) = \frac{y_{I_l}(n)}{\sqrt{\hat{\sigma}_{I_l}^2(n)}} \quad (7)$$

The new time-series  $\mathbf{y}_{R_{l_{\text{new}}}}$  and  $\mathbf{y}_{I_{l_{\text{new}}}}$  are then used for model order selection/estimation. The value of the smoothing factor  $\lambda$  is tuned using particle swarm optimization [11]. The fitness function selected to be minimized is

$$J = \sum_{n=1}^N [y_{R_{l_{\text{new}}}}^2(n) + y_{I_{l_{\text{new}}}}^2(n)] \quad (8)$$

## III. SIMULATIONS

### A. Simulation Study I

The first simulation paradigm consists of generating images based on MVAR models in order to examine the effect of heteroscedasticity. We generated 1700 IQ-like images of dimension  $N \times L$ , where  $N = 1000$  is the total number of sample points in the axial direction, and  $L = 128$  is the number of lines in the lateral direction. Each line was modeled as a stable, two-dimensional ( $M = 2$ ), MVAR(5) process,

$$\mathbf{y}_l(n) = \begin{bmatrix} y_{R_l}(n) \\ y_{I_l}(n) \end{bmatrix} = \sum_{k=1}^5 \mathbf{A}_k \mathbf{y}_l(n-k) + \boldsymbol{\varepsilon}_l(n), \quad (9)$$

where the subscript  $l$  denotes the  $l^{\text{th}}$  line ( $l = 1 \dots L$ ),  $\mathbf{y}_l(n)$  consists of the real and imaginary components of the  $l^{\text{th}}$  line at time  $n$ , and  $\boldsymbol{\varepsilon}_l(n)$  is an heteroscedastic white Gaussian noise vector. The  $l^{\text{th}}$  line can be expressed in complex form as

$$y_{C_l}(n) = y_{R_l}(n) + i \cdot y_{I_l}(n), \quad (10)$$

where  $\mathbf{Y}_{C_l} = [y_{C_l}(1) \dots y_{C_l}(N)]^T \in \mathbb{C}^{N \times 1}$ . The noise  $\boldsymbol{\varepsilon}_l(n)$  can also be seen as a complex Gaussian random variable,

$$\boldsymbol{\varepsilon}_{C_l}(n) = \varepsilon_{R_l}(n) + i \cdot \varepsilon_{I_l}(n), \quad (11)$$

where  $\mathbf{E}_{C_l} = [\boldsymbol{\varepsilon}_{C_l}(1) \dots \boldsymbol{\varepsilon}_{C_l}(N)]^T \in \mathbb{C}^{N \times 1}$ . The final simulated image is  $\mathbf{I} = [\mathbf{Y}_{C_1} \dots \mathbf{Y}_{C_L}] \in \mathbb{C}^{N \times L}$ . Heteroscedasticity was introduced in  $\mathbf{E}_C = [\mathbf{E}_{C_1} \dots \mathbf{E}_{C_L}]$  by modulating the real and imaginary parts of an homoscedastic complex Gaussian image  $\mathbf{W}_C = [\mathbf{W}_{C_1} \dots \mathbf{W}_{C_L}] \in \mathbb{C}^{N \times L}$  by an envelope image  $\mathbf{H}$

$$\text{Re}(\mathbf{E}_C) = \text{Re}(\mathbf{W}_C) \odot \mathbf{H}, \quad \text{Im}(\mathbf{E}_C) = \text{Im}(\mathbf{W}_C) \odot \mathbf{H}, \quad (12)$$

where  $\mathbf{H} \in \mathbf{R}_{>0}^{N \times L}$  and  $\odot$  denotes the Hadamard product.  $\mathbf{H}$  was created using a linear combination of Gaussian and Laplacian kernels with different weights, sizes and standard deviations. The number of kernels, as well as the position of the center of each kernel on the image was chosen randomly.

### B. Simulation Study II

For this simulation study, we applied both conventional and the proposed methodology on phantom and in vivo IQ images. Specifically, we examined,

- *Dataset 1*: The cyst phantom of Field II [12].
- *Dataset 2*: The focused imaging dataset of hyperechoic cyst and point scatterers [13].
- *Dataset 3*: The human heart parasternal long axis view dataset [13], [14].
- *Dataset 4*: The in vivo carotid longitudinal-section dataset [13], [15].

Datasets 2,3,4 were provided by the Ultrasound Toolbox [13].

## IV. RESULTS AND DISCUSSION

For comparison purposes all images were log compressed and adjusted in a dynamic range of 60dB. The resulting images are denoted with the symbol  $\tilde{\cdot}$ . In the first simulation case, the ground truth was known. Therefore, the deconvolution performance of the proposed and the conventional MVAR estimation technique were quantified using the well-known Peak-to-Signal Noise Ratio (PSNR) expressed as

$$\text{PSNR}_{\text{real}} = 10 \log_{10} \left( \frac{255^2}{\text{MSE}_{\text{real}}} \right), \quad [13a]$$

$$\text{MSE}_{\text{real}} = \frac{1}{L \cdot N} \sum_{l=1}^L \sum_{n=1}^N [\tilde{\mathbf{E}}_C(n, l) - \hat{\mathbf{I}}(n, l)]^2, \quad [13b]$$

where  $\hat{\mathbf{I}}$  is the log compressed deconvolved image. We also calculated the quantity  $\text{PSNR}_{\text{est}}$ , where instead of  $\tilde{\mathbf{E}}_C$  in (13b), we used the image  $\tilde{\mathbf{I}}$ . For the second simulation set,  $\text{PSNR}_{\text{est}}$  was the main metric of performance, since  $\tilde{\mathbf{E}}_C$  was not known.

### A. Simulation Study I

The performance of both conventional and proposed techniques was found to be dependent on the coefficient of variation ( $CV$ ) of the modulating envelope image  $\mathbf{H}$  (Fig.1a). Herein,  $CV$  was defined as the standard deviation of each line's intensity divided by its mean intensity and averaged over all lines.  $CV$  describes the extent of variability in relation to the mean and can be used to quantify the magnitude of heteroscedasticity in the data. An image with very low  $CV$  could

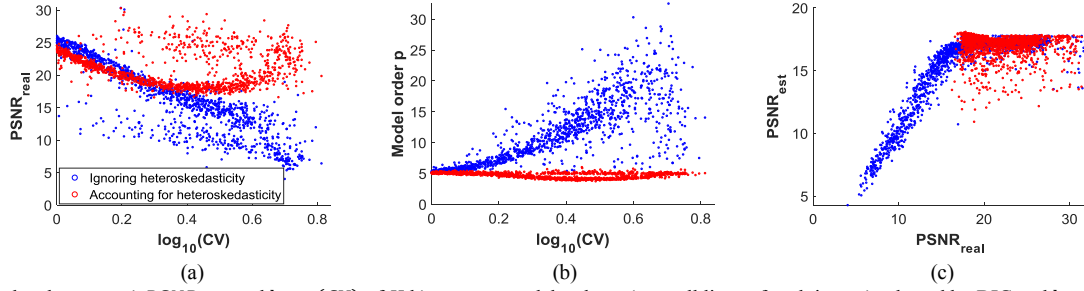


Fig. 1. Scatterplots between a)  $PSNR_{real}$  and  $\log_{10}(CV)$  of  $\mathbf{H}$  b) average model order  $p$  (over all lines of each image) selected by BIC and  $\log_{10}(CV)$  of  $\mathbf{H}$  (note that all lines in an image were simulated using an order  $p = 5$ ) and c)  $PSNR_{real}$  and  $PSNR_{est}$ . The blue circles correspond to the case where the conventional MVAR technique was applied, ignoring heteroscedasticity. The red circles correspond to the proposed approach, where heteroscedasticity was taken into account.

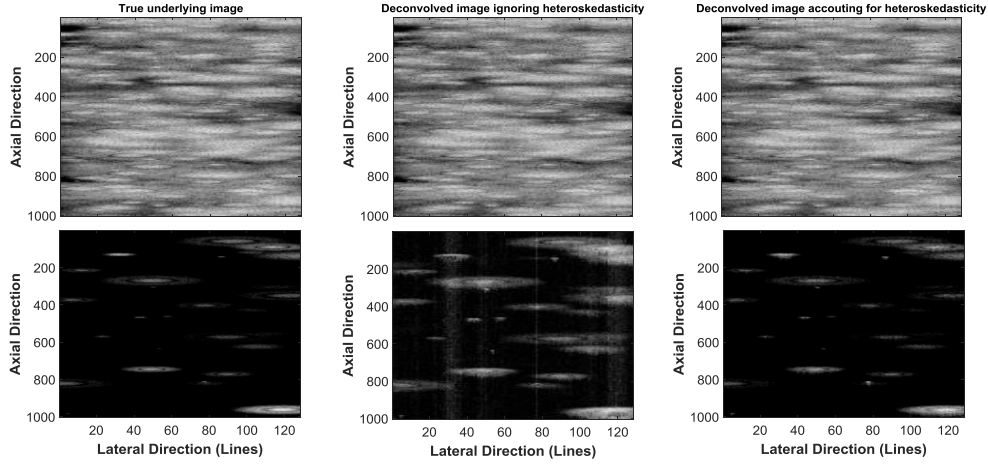


Fig. 2. Deconvolution results based on the conventional MVAR estimation technique (middle panel), where heteroscedasticity is not accounted for, and the proposed approach (right panel). The true underlying image  $\tilde{\mathbf{E}}_C$  is depicted in the left panel. The top and bottom panels correspond to the case where the  $CV$  of the modulating envelope image  $\mathbf{H}$  is  $\log_{10} CV = 0.037$  and  $0.678$ , respectively. For the top and bottom panels the values of  $[PSNR_{real}, PSNR_{est}]$  are  $[26.90, 17.49]$  vs  $[24.22, 17.39]$  and  $[11.39, 11.09]$  vs  $[20.41, 17.73]$  for the conventional vs proposed approach, respectively.

either be an almost homoscedastic Gaussian noise image or a very dense image with high mean intensity and low variability. The negative effect of increased  $CV$  was observed mainly in the case of the conventional MVAR estimation technique. Based on Fig. 1a, by taking into account the heteroscedasticity in the data, our proposed approach led to higher  $PSNR_{real}$  values as the  $CV$  of the image increased. Model order selection was also affected by heteroscedasticity. A large  $CV$  led BIC into selecting high  $p$  values and therefore complex models that overfit the data (Fig. 1b). The presence of heteroscedasticity results in large variance residuals that dominate the global estimate  $\hat{\Sigma}$  (4) and significantly reduce the effective sample size. Consequently, when heteroscedasticity is ignored BIC selects erroneously overdetermined models. In contrast, following our proposed approach, the MVAR residuals become more homoskedastic, and hence, BIC selects more parsimonious models with a model order similar to the true one ( $p = 5$ ). Fig. 2 illustrates the deconvolution results from two different images where the  $CV$  of  $\mathbf{H}$  was  $\log_{10} CV = 0.037$  and  $0.678$ , respectively. For a low  $CV$  both approaches efficiently approximated the true underlying image  $\tilde{\mathbf{E}}_C$ , with the conventional technique achieving slightly higher  $PSNR_{real}$  values. For a moderate to high  $CV$ , the proposed approach exhibited superior performance due to the presence of significant heteroscedastic effects.

In reality,  $PSNR_{real}$  cannot directly be estimated, therefore  $PSNR_{est}$  is used as a metric of performance. For comparison purposes we illustrate the relationship between  $PSNR_{real}$  and

$PSNR_{est}$  in Fig. 1c. Overall, we observed a linear dependence between these two quantities. However,  $PSNR_{est}$  exhibited a plateau for values of  $PSNR_{real}$  over 16, and this is expected since the point of reference is the convolved image  $\mathbf{I}$  and not the true underlying image  $\tilde{\mathbf{E}}_C$ . The plateau value for  $PSNR_{est}$  is theoretically equal to the  $PSNR$  obtained by computing the  $MSE$  between  $\mathbf{I}$  and  $\tilde{\mathbf{E}}_C$ .

Regarding runtime, the conventional approach required  $0.566 \pm 0.042$ s for each image, whereas the proposed technique was slightly slower (due to the particle swarm optimization of the smoothing factor  $\lambda$  of (6) – see Section II.B) with an execution time of  $1.059 \pm 0.117$ s per image (Intel Core i7-7500U@2.70GHz, 16GB RAM).

### B. Simulation Study 2

The deconvolution results of this simulation study can be found in Fig. 3. To quantify the performance of both conventional and proposed approaches we computed the  $PSNR_{est}$  on each deconvolved image. In all cases, taking into account heteroscedasticity led to higher  $PSNR_{est}$  values (and therefore improved contrast and resolution) compared to the case where heteroscedasticity was ignored.

## V. CONCLUSIONS

The main goal of this study was to elucidate the effects of volatility clustering in medical ultrasound imaging and provide a robust as well as fast deconvolution algorithm. The superiority

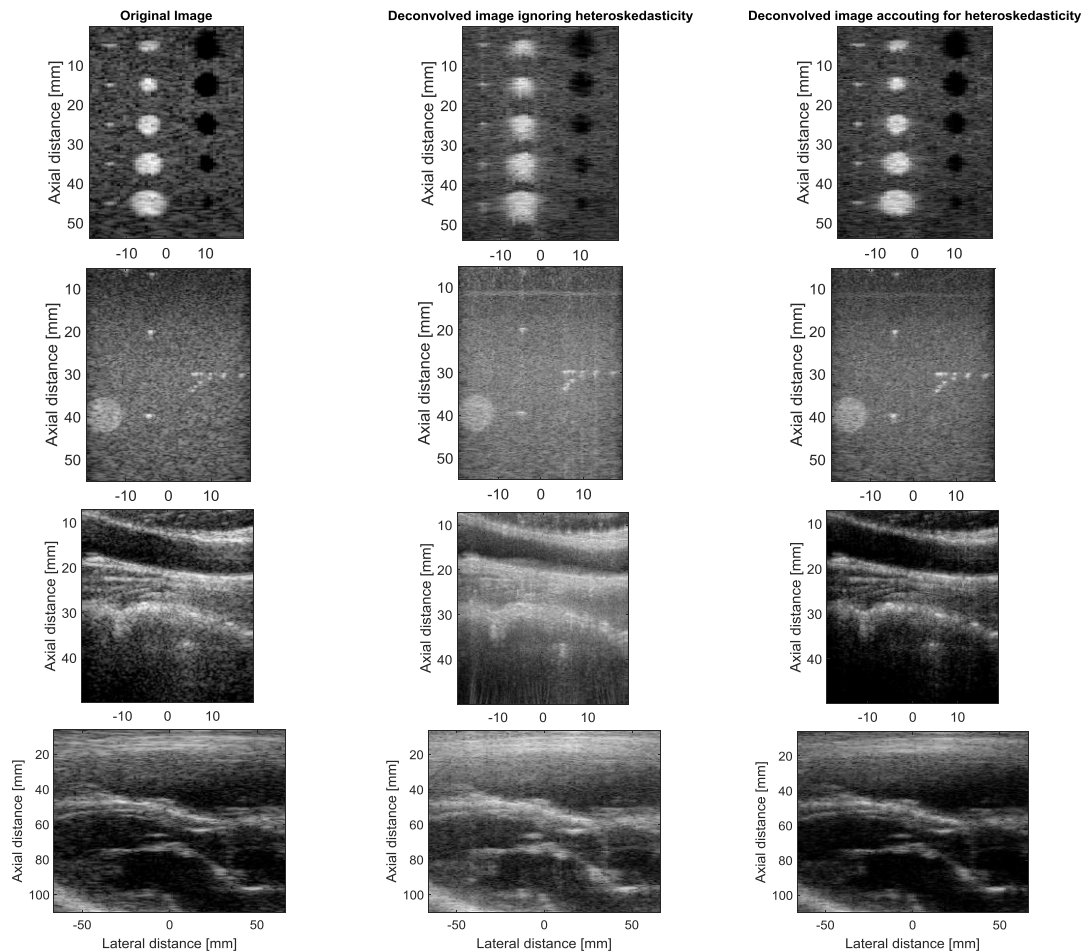


Fig. 3. Deconvolution results based on the conventional MVAR estimation technique (middle panel) and the proposed approach (right panel). The original B-mode IQ image  $\tilde{I}$  is depicted in the left panel. The 1<sup>st</sup>, 2<sup>nd</sup>, 3<sup>rd</sup> and 4<sup>th</sup> row correspond to Dataset 1, 2, 3 and 4, respectively. From top to bottom, the  $PSNR_{est}$  for the conventional technique was 17.60, 16.36, 14.72 and 14.94. The values of  $PSNR_{est}$  for the proposed approach were 18.67, 18.82, 15.64 and 18.75.

of the proposed methodology under highly heteroscedastic environments justifies further investigation. Future work will involve the extension of the proposed model into a time-varying context in order to account also for pulse distortions and attenuation-dependent frequency shifts.

#### ACKNOWLEDGMENT

The authors thank Dr. Martin Mienkina of GE Healthcare Austria for his valuable advice and assistance. This work has been supported by the COMET-K2 Center of the Linz Center of Mechatronics (LCM) funded by the Austrian federal government and the federal state of Upper Austria.

#### REFERENCES

- [1] J. A. Jensen, "Estimation of Pulses in Ultrasound B-Scan Images," *IEEE Trans. Med. Imaging*, vol. 10, no. 2, pp. 164–172, 1991.
- [2] J. A. Jensen, J. Mathorne, T. Gravesen, and B. Stage, "Deconvolution of in-vivo ultrasound B-mode images," *Ultrason. Imaging*, vol. 15, no. 2, pp. 122–133, 1993.
- [3] J. A. Jensen, "Real time deconvolution of in-vivo ultrasound images," *IEEE Int. Ultrason. Symp. IUS*, pp. 29–32, 2013.
- [4] E. von Lavante and J. A. Noble, "Improving the contrast of breast cancer masses in ultrasound using an autoregressive model based filter.," *Med. Image Comput. Comput. Assist. Interv.*, vol. 10, no. Pt 1, pp. 153–60, 2007.
- [5] J. Zielinski, N. Bouaynaya, and D. Schonfeld, "Two-dimensional ARMA modeling for breast cancer detection and classification," *Int. Conf. Signal*

- Process. Commun. SPCOM*, pp. 1–4, 2010.
- [6] G. Chandler, "Order selection for heteroscedastic autoregression: A study on concentration," *Stat. Probab. Lett.*, vol. 80, no. 23–24, pp. 1904–1910, 2010.
- [7] H. Lütkepohl, *New introduction to multiple time series analysis*. Springer Science & Business Media, 2005.
- [8] G. Schwarz, "Estimating the dimension of a model," *The Annals of Statistics.*, vol. 6, no. 2, pp. 461–464, 1978.
- [9] S. De Waele and P. M. T. Broersen, "Order Selection for Vector Autoregressive Models," *IEEE Transactions on Signal Processing*, vol. 51, no. 2, pp. 427–433, 2003.
- [10] L. Faes, S. Erla, and G. Nollo, "Measuring connectivity in linear multivariate processes: definitions, interpretation, and practical analysis," *Computational and Mathematical Methods in Medicine.*, vol. 2012, pp. 1–18, 2012.
- [11] J. Kennedy, "Particle swarm optimization," in *Encyclopedia of machine learning*, Springer, pp. 760–766, 2011.
- [12] J. A. Jensen, "Field: A program for simulating ultrasound systems," in *10th Nordiccaltic Conference on Biomedical Imaging*, vol. 4, supplement 1, Pt 1, pp. 351–353, 1996.
- [13] A. Rodriguez-Molares *et al.*, "The ultrasound toolbox," *IEEE Int. Ultrason. Symp. IUS*, pp. 1–4, 2017.
- [14] H. Liebgott, A. Rodriguez-Molares, F. Cervenansky, J. A. Jensen, and O. Bernard, "Plane-wave imaging challenge in medical ultrasound," *IEEE Int. Ultrason. Symp. IUS*, pp. 1–4, 2016.
- [15] O. M. H. Rindal, S. Aakhus, S. Holm, and A. Austeng, "Hypothesis of improved visualization of microstructures in the interventricular septum with ultrasound and adaptive beamforming," *Ultrasound Med. Biol.*, vol. 43, no. 10, pp. 2494–2499, 2017.